International Journal of Mechanical Design and Materials Science

Volume 1, Issue 2 2025

An integrated geometric-graph-theoretic method for depicting origami structures and the truss frameworks that go with them

Tairan ,Fu. Department of Energy and Power Engineering, Tsinghua University, Beijing, 100084, China

Research Article

Date of Submission: 10-03-2025 Date of Acceptance: 19-03-2025 Date of Publication: 1-04-2025

Abstract: Numerous intriguing uses for origami have been found in science and engineering. In order to create an inventive origami structure with the necessary qualities, appropriate representations and assessment of crease patterns are crucial. However, scientists and engineers that use origami in a variety of domains often face this difficulty. Graph products are a good option for the creation of crease patterns since the majority of useful origami structures have repeating unit cells. In order to depict crease patterns and the related truss frameworks of origami structures, we will use both directed and undirected graph products. We show that an origami crease pattern may be precisely defined by a certain graph product of independent graphs because the pattern can be thought of as a collection of directionless crease lines that meet the foldability criterion. It turns out that this combined geometric-graph-theoretic approach may be successfully used to the creation of various crease patterns and provide appropriate node and element numbering. Additionally, the provided technique improves configuration processing for geometric, kinematic, or mechanical study on origami structures by helping to create the required matrices and models of origami structures.

Keywords: Repetitive fold patterns, pin-jointed structures, directed graphs, origami patterns, and graph theory

Introduction

Folding 2D materials, such a flat sheet of paper, into 3D items with desired forms is the art of origami. Since the early 1980s, origami has developed into a thriving scientific subject that links numerous fields and produces a vast array of novel designs with a wide range of uses. The fast growth of origami as a new area of study has been aided in recent years by creative engineering and mathematics research. Mathematicians, engineers, and scientists are particularly interested in the intriguing mechanical characteristics of origami structures [1–5]. For example, in the fields of fashion, architecture, medicine, and engineering—from airbags to flexible electronics to deployable space constructions—the structural rigidity and geometric shape-shifting capabilities of some origami structures have garnered significant interest [1, 6, 7]. Tree theory, computational origami theory, optimization techniques for stiff origami, and geometric mechanics of origami structures have all seen significant theoretical advancements [8]. Recently, 2D sheets have been folded along well planned creases to create reprogrammable structures utilizing origami methods. Because their characteristics are neatly tied to an adjustable crease pattern, origami-inspired structures have a major benefit in terms of increased performance flexibility [3]. Research has been done on origami-inspired structures using the non-periodic Resch pattern and the periodic Miura pattern [9]. The Miura fold pattern has been shown to have a negative in-plane Poisson's ratio. According to Wei et al. [8], regardless of material qualities, the in-plane and out-of-plane Poisson's ratios have the same magnitude but the opposite sign. Additionally, the Resch pattern's exceptional folding technique has been shown to have a significant load-bearing capacity. Kuribayashi et al. [10] suggested an origami-inspired stent graft and introduced the six-fold origami design to biomedical engineering. Hunt et al. [11] demonstrated origami designs with twist buckling and investigated the buckling process of a thin cylindrical shell under torsion. Additionally, they looked at the corresponding truss models' critical buckling loads and buckling processes.

It is important to note that modeling and in-depth examination of the structures are required when either creating a new pattern or examining certain aspects of these origami-inspired constructions. For origami structures, configuration processing, also known as pre-processing, is crucial.

There aren't many research that provide strong and comprehensive configuration processing techniques for these novel designs. Graph-theoretical techniques for creating structural configurations and numerical models have been developed by Kaveh and Koohestani [12, 13].
Graph Products for the Representation of Crease Patterns. Given that an origami crease pattern can be considered to be a set of directionless crease lines which satisfy the foldability condition [16, 17], here we demonstrate that the pattern can be exactly expressed by a specific graph product of independent graphs. By definition, a *graph* S consists of a set of nodes (or vertices) N(S), and a set of members (or edges) M(S) [18]. A relation of incidence for the nodes and members of a graph is denoted by an
adjacency matrix A(S). The matrix A(S) of an undirected graph with n nodes is an $n \times n$ symmetric matrix,

whose entry $A_{ij}(S)$ in the ith row and jth column is given by

$$A_{ij} \quad \begin{cases} 1 & \text{if node } i \text{ is connected to node } j \text{ by a member} \\ 0 & \text{otherwise} \end{cases} \tag{1}$$

A graph is called to be a directed graph, provided that orientations are assigned to its members [14]. Then, a

modified adjacency matrix $\bar{A}(S)$ for this directed graph with n nodes can be defined as

$$\bar{A}_{ij} \quad \begin{cases} 1 & \text{if node } i \text{ is connected to node } j \text{ and directed from node } i \text{ to node } j \\ 0 & \text{otherwise} \end{cases} \tag{2}$$

In Eq. (2), the marix $\bar{A}(S)$ is an $n \times n$ nonsymmetric matrix.

Cartesian product of undirected graphs

Many origami structures with degree-4 vertices (e.g., the Miura-ori) have symmetric patterns and thus can be considered to be *the Cartesian product* of simple graphs K and H, expressed as K□H. In fact, the Cartesian product of subgraphs K and H can be formed by taking copies of H for all the nodes of K and joining these copies [13, 18, 19]. By using the Boolean operation for the Cartesian product, we can denote the corresponding adjacency matrix A(K□H) as

$$A(K\square H) = A(K) \otimes I_{n_H} \oplus I_{n_K} \otimes A(H) \quad (3)$$

in which I_{n_k} is the $n_k \times n_k$ identity matrix, n_k is the number of nodes of the graph K, I_{n_h} is the $n_h \times n_h$ identity matrix, n_h is the number of nodes of the graph H, and $\otimes$ describes the Kronecker product of the matrices. For example, the Cartesian product of two simple graphs $K=P_2$ and $H=P_3$ (Fig. 1a-b) is illustrated in Fig. 1(c). Note that a graph P is known as a *path graph* whose nodes and members lie on a single straight line [19]. Consequently, the adjacency matrix A(K□H) for the generated graph shown in Fig. 1(c) can be directly computed from Eq. (3), given by

$$A(K\square H)= \begin{bmatrix} 0 & 1 & 0 & 1 & 0 & 0 \\ 1 & 0 & 1 & 0 & 1 & 0 \\ 0 & 1 & 0 & 0 & 0 & 1 \\ 1 & 0 & 0 & 0 & 1 & 0 \\ 0 & 1 & 0 & 1 & 0 & 1 \\ 0 & 0 & 1 & 0 & 1 & 0 \end{bmatrix} \quad (4)$$

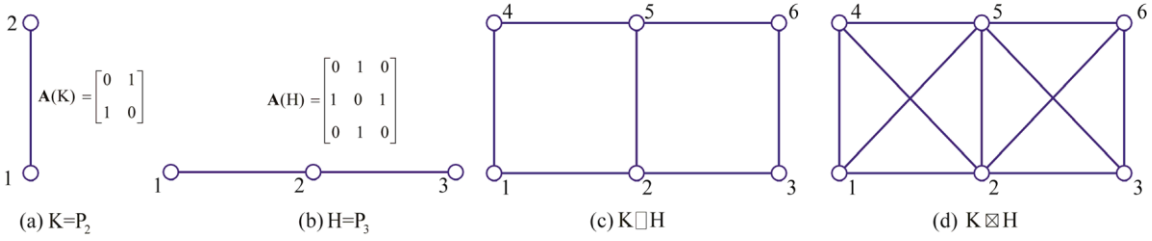


Figure 1 The Cartesian product and strong Cartesian product of two simple graphs

Strong Cartesian product of undirected graphs

The strong Cartesian product of two undirected graphs K and H is given by K⊠H [20], which is another type of

Boolean operation. The nodes of graph K are i_k, $j_k \in$ N(K), and a i_k j_k member if it is denoted by M(K)

connected by two nodes and j_k . Similarly, we denote that a i_h j_h □ is connected by two i_k member M(H)

nodes i_h , j_h □ of graph H. Then, for different i □ (i_k , and j □ (j_k , of the strong N(H) nodes i_h) j_h) Cartesian

product K⊠H, it satisfies

□if i_k □ j_k , and i_h j_h □ M(H)

Nodes *i* and *j* are connected by a member □elsei i □ j , and i j □ M(K) (5)
f

□ h h k k
□ i_k j_k □ M(K), and i_h j_h □ M(H)
□□elseif

In Eq. (5), the i □ (i_k , i_h), j □ (j_k , j_h) □ N(K) □ N(H) . Thus, the adjacency matrix nodes A(K⊠H) of the strong

Cartesian product is computed by

A(K⊠H) = A(K) □ I_n □ I_n □ A(H) □ A(K) □ (6)
A(H)

h k

For example, Fig. 1(d) plots the strong Cartesian product of the above-mentioned graphs $K=P_2$ and $H=P_3$. In this figure, the diagonal members exist because the third condition in Eq. (5) is satisfied. In fact, the involved
adjacency matrix A(K⊠H) for the graph shown in Fig. 1(d) can be obtained from Eq. (3), written as

A(K⊠H)= □1 0□ □ 0 1 0 □ □0 1□ □ 1 0 1 □ □1 0□ □0 1 0 1 1 0□ (7)
□ 1 0 1 □ □ □ 1 0 1 0 0 1
□ 0 1 0 0 1 1
□ 0 1 0 1 1 0
□1 1 1 1 0 1□

Directed graph products

Type I directed graph product, which is (□) and proposed by Kaveh and Koohestani denoted by 1 [13], is

utilized to generate triangular patterns for multi-fold origami. For two directed graphs K and H, any two nodes

$i \square (i_K, i_H$ and $j \square (j_K$, are connected if one of these six conditions $i_K \square i_H\ j_H \square$ M(H); $j_H)$ holds: (i) j_K, (ii)

$i_K \square j_K j_H i_H \square$ M(H); $i_H \square i_K\ j_K \square$ M(K); $i_H \square j_K\ i_K \square$ M(K); $i_K\ j_K \square i_H\ j_H \square$ M(H), (iii) j_H, (iv) j_H, (v) M(K), ;

(vi) $j_K\ i_K \square j_H i_H \square$ M(H). It should be noted that, for directed $i_K\ j_K \square$ holds if and only if M(K), graphs, M(K)

node i_K is connected to node j_K and directed from to node j_K. node i_K

To effectively generate the directed products of graphs K and H, we can also concern the corresponding adjacency matrix $A(K (\square)_1 H)$, given by

$$A(K(\square)_1 H) = A(K) \square I_n \quad \square I_n \qquad T \qquad (H\ (8)$$
$$)$$
$$\square\ A(H) \square\ A(K) \square\ A(H) - T$$
$$\square\ A \qquad (K) \otimes$$
$$A$$

h *k*

where $\overline{A}(K)$ and $\overline{A}(H)$ denote the adjacency matrices of undirected graphs of K and H, and

$\overline{A}(H)$ can be obtained from Eq. (2). Some examples of this product are plotted in Fig. 2, whereas the graphs S_1,

S_2 and S_3 are directed graphs. The member 23 of the directed graphs S_2 and S_3 in Fig. 2(b-c) has opposite directions, which indicates the manner for generating the diagonal members.

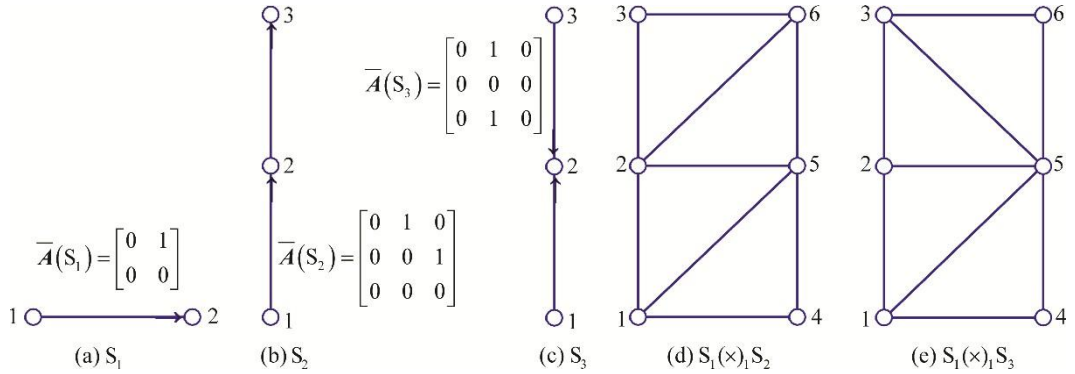


Figure 2 Type I directed graph products of several graphs S_1, S_2 and S_3

Algebraic weighted graphs

Graph products can generate tessellations with new connectivity [13, 15]. However, certain geometric parameters such as angles between edge lines and the lengths of edges, which are not important in graph theory, have not been integrated into a conventional graph-theoretic approach [21-23]. In fact, these parameters are important in the developability, flat-foldability, or rigid-foldability of an origami pattern [24-26], and thus they should be somehow incorporated.
In this case, an integrated geometric-graph-theoretic framework is proposed, to include both geometry and connectivity in the mathematical notation. Weighted graphs, which may be either directed or undirected, are utilized to incorporate the lengths of crease lines. In other words, each edge of a graph is associated with a numerical value, called a weight [22]. Then, an entry $A_{ij}(S)$ in the *i*th row and *j*th column of a weighted graph S is defined as follows

$$A_{ij}(S) = \begin{cases} l_{ij} & \text{if node } i \text{ is connected to node } j \text{ by a member} \\ 0 & \text{otherwise} \end{cases} \quad (9)$$

where l_{ij} denotes the length of the involved crease line. To effectively distinguish the directions of the creases for an origami pattern, crease (i, j) in Eq. (9) is denoted for a mountain fold, (j, i) for a valley fold. while -1 1

For a non-weighted graph l_{ij} should be replaced by unity. Thereafter, Eq. (9) reduces to either Eq. (1) or Eq. (2). In addition, zero weights should be assigned to the members which need to be removed. In practice, the sum of absolute weights of a graph can be a measure of the complexity of crease processing.

Furthermore, a turning angle between two adjacent edge lines is defined as the weight of the common node, to describe the 2D geometric configuration of the subgraphs of an origami pattern. That is, the i-th entry $N_i(S)$ of a weighted graph S in 2D space is defined as

$$N_i(S) = \theta_i \quad (10)$$

where the turning angle $-180° < \theta_i \leq 180°$ is the directed angle (the counterclockwise direction is positive [27]) from vector $\overrightarrow{N_{i-1}N_i}$ to vector $\overrightarrow{N_iN_{i+1}}$. The notation in Eq. (10) is specifically for path graphs and a general 2D graph, because it can neatly describe the orientation of the graph in 2D space. Note that the turning angles θ_i of the two endpoints of an unclosed graph can be evaluated with respect to $+x$ axis.

In more general cases, nodal coordinates should be associated with a specific node to accurately describe the origami pattern and its subgraphs in 3D space. Then, the i-th entry $N_i(S)$ of a weighted graph S in 3D space is defined as

$$N_i(S) = [x_i \; y_i \; z_i]^T \quad (11)$$

where x_i, y_i, and z_i denote the coordinates of node i in 3D space.

Further operations employed for graph products

We have introduced several types of undirected/directed graph products, which are capable of generating a series of origami patterns. Nevertheless, other operations can be further employed to enhance this capability. These

additional operations include intersection (e.g., $S_1 \cap S_2$), ring sum (e.g., $S_1 \oplus S_2$) and union (e.g., $S_1 \cup S_2$). They are useful for subtracting or adding groups of nodes and/or members. Furthermore, we can define other operations to strengthen these capabilities for the formation of complicated origami patterns. Complementary examples will be presented in the next section.

Note that the operands are assumed to have the same number of nodes. Then, the involved matrices of the resulted graph can be easily computed from the matrices of the operands. Moreover, a node should be deleted, on condition that it is left non-connected to the other nodes [18].

Examples of Origami Structures

In this section, different types of origami structures are developed using the introduced integrated geometric-graph-theoretic framework.

Crease pattern and truss framework of the Miura-ori

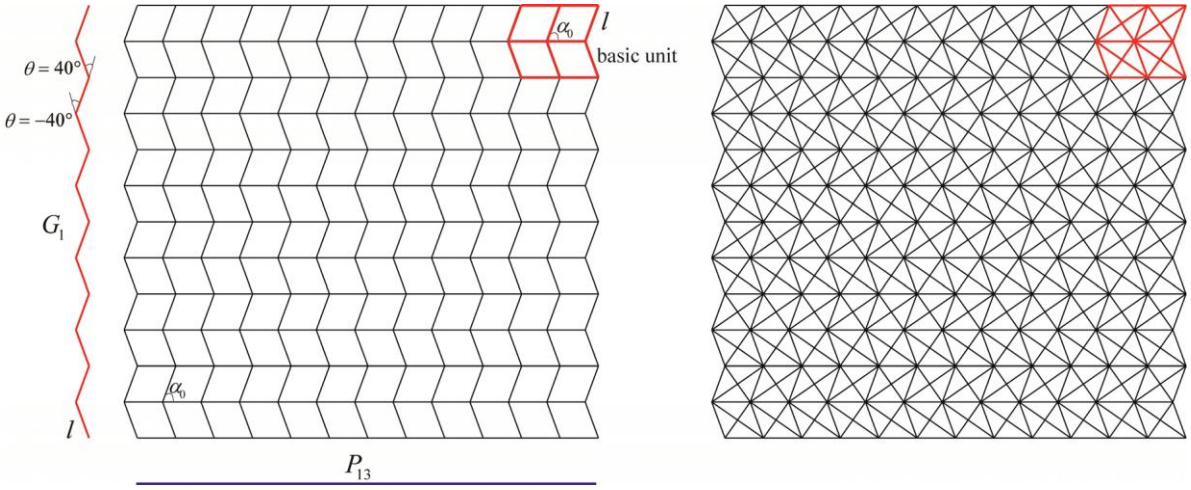
Figure 3(a) shows the crease pattern of the Miura-ori with 6×6 basic units. In fact, it can be generated from the

Cartesian product of a straight line P_{13} and a piecewise parallel polylines G_1. As the acute angle and edge lengths

of the parallelogram for the basic unit in the presented example are $\alpha_0 = 70°$ and $l_h = l_v = l$, respectively the

turning angle between the adjacent edge lines of $\rho_i = (180° - 2\alpha_0) = 40°$. All the graph G_1 is members of

graphs P_{13} and G_1 have the same length, l. Moreover, the truss framework corresponding to the Miura-ori, shown in Fig. 3(b), is the strong Cartesian product of graphs P_{13} and G_1. This origami-based truss structure has 169 nodes and 600 truss members. First-order analysis shows that this equivalent truss structure is both kinematically
and statically indeterminate, as the rank of the corresponding 507×600 equilibrium matrix is 456.



(a) P_{13}□G_1 (b) P_{13} □ G_1

Figure 3 Crease pattern and truss framework of the Miura-ori, respectively, denoted by: (a) the Cartesian product, and (b) the strong Cartesian product of two graphs

Numerical simulation on these origami structures is also performed, to predict the folding motion. Note that the origami model shown in Fig. 3(a) is kinematically investigated using the internal mechanism mode extracted from the equilibrium matrix and the nonlinear prediction-correction method [28, 29]. Besides, the equivalent truss model shown in Fig. 3(b) is analyzed using ABAQUS, whereas each vertex denotes pin-joint node and each member is simulated by a three-node quadratic displacement truss element (to avoid the instability and undesirable deflection of the truss member) [29]. Displacement-based static analysis is utilized for following the folding process, and the geometric nonlinearity is considered. Figure 4 shows typical configurations of the origami model and the corresponding truss framework during transformations. Both structures exhibit similar configurations and transformations during the folding process. Note that the folding is verified to be feasible and

approximately rigid-foldable, as the maximum strain of the truss members $1.5\acute{}10^{-3}$ along the is less than

whole process. This rigid-folding behavior is in good agreement with the results reported by recent studies [17, 29, 30]. Thus, both structural models can simulate the single degree-of-freedom folding behavior of the Miura origami tessellation. Importantly, this Miura-ori structure shows satisfactory folding ratio, whereas the ratio of

the folded area to the unfolded one is about 0.0451.

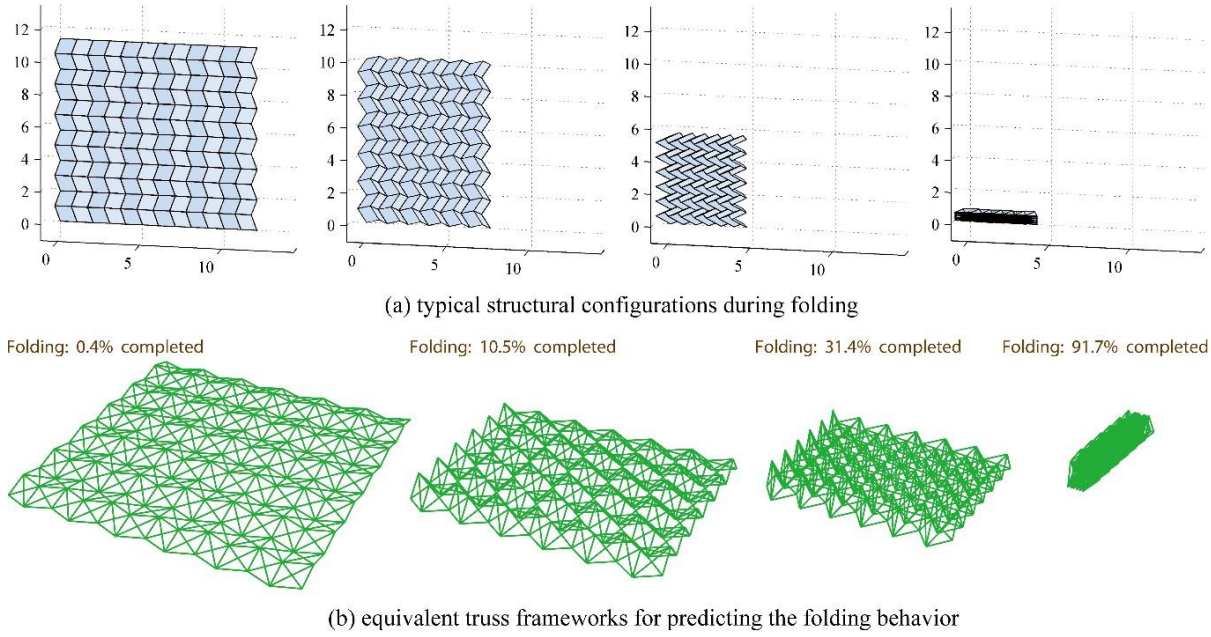
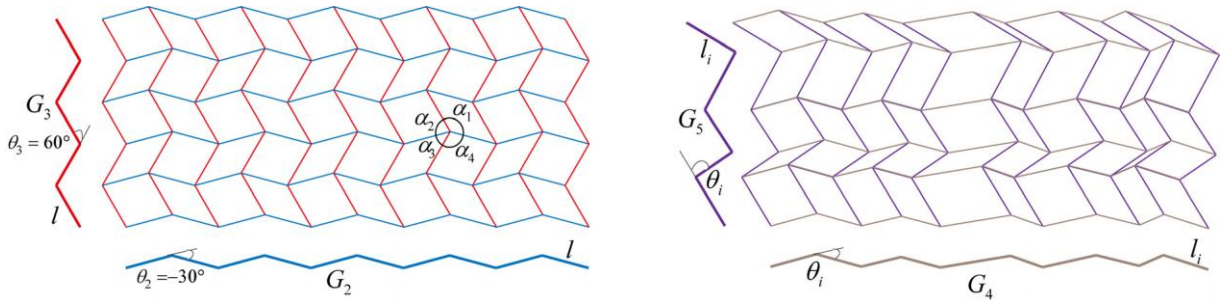


Figure 4 Rigid folding of an origami model with Miura pattern

Representation of different degree-4 origami structures

The design of appropriate crease patterns is the first step in the development of innovative origami structures with desired characteristics. However, generally this is a challenge encountered by not only origami artists, but also by scientists and engineers who exploit origami patterns in various fields (Tachi [9]; Sareh and Guest [17]). In fact, an integrated mathematical framework for the development of such patterns can be useful as a representational tool, and can inform computer programs generating structural concepts. Here, some degree-4 origami patterns different from the classical Miura-ori are represented by the Cartesian products of different undirected graphs (Fig. 5).



(a) $G_2 \square G_3$ (b) $G_4 \square G_5$

Figure 5 Crease patterns of two different degree-4 origami patterns obtained from the Cartesian products of appropriate subgraphs

The subgraphs G_2 and G_3 shown in Fig. 5(a) are the longitudinal and transverse polylines [16, 17, 31] of the

origami tessellations, respectively, where $\square_i$ (G_2) $\square\square_i$ (G_3) $\square$ $\square 60\square$, and the length (weight) of $\square 30\square$, each edge

line is $l_{ij} = l$. As the corresponding Cartesian product contains only two types of four-fold vertices, it allows us to determine the flat-foldability in a much easier way. Interestingly, this graph product, which is taken as a modified Miura origami, has been verified to be flat-foldable [25, 31]. As expected, the angles at each four-fold vertex satisfy the following condition

$$\square_1 \square\square_3 \square\square_2 \square\square_4 \square 180\square \quad (12)$$

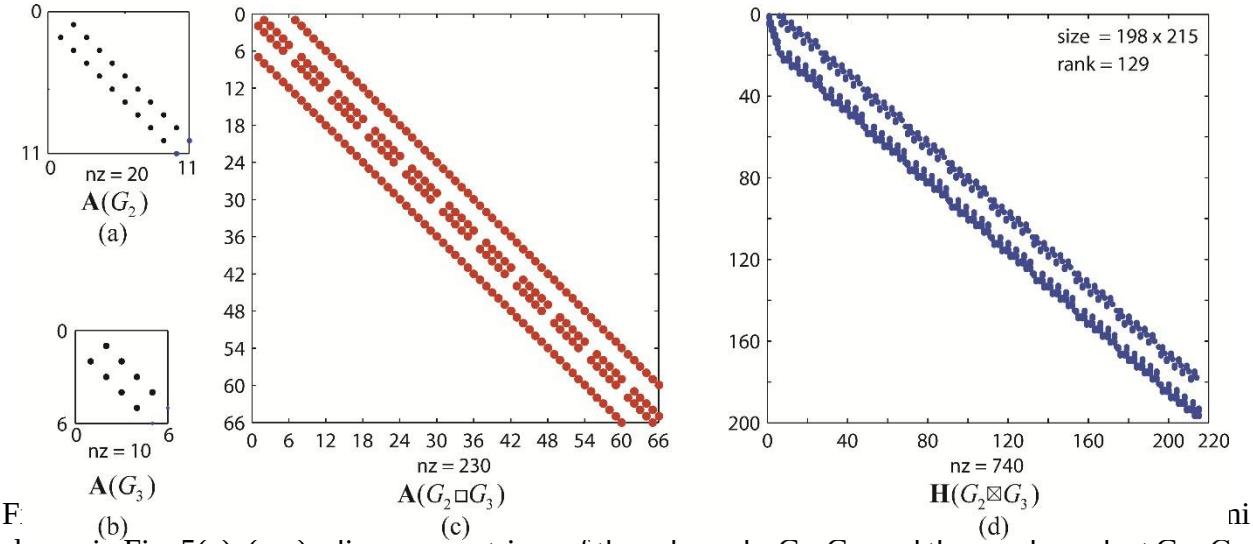
$\square\square_i \square 360\square$, and $i \square 1$

Eq. (12) can guarantee the local flat-foldability for each vertex of a four-fold origami pattern [25, 31], and it is a necessary condition for the global foldability [32, 33]. For instance, the four angles illustrated in Fig. 5(a) are respectively $\square_1 \square 135\square$, $\square_2 \square 75\square$, $\square_3 \square 45\square$, and $\square_4 \square 105\square$. Note that the truss structure for this model can be

directly obtained from the strong Cartesian product of graphs G_2 and G_3.

On the other hand, our method can be extended to represent various four-fold origami patterns. Fig. 5(b) shows a more general four-fold origami model than the Miura-ori. It is obtained from the Cartesian product of the graphs G_4 and G_5, which are two arbitrary polylines. On condition that the rigid-foldability or the flat-foldability of the structure is guaranteed by the reported foldability conditions [25, 31, 32], the proposed method provides an effective way for developing different four-fold origami structures. For example, as far as the local flat-foldability of the origami pattern shown in Fig. 5(b) is concerned, only the angles associated with a small number of vertices need to be evaluated by Eq. (12), because the origami pattern obtained from subgraphs contain periodic cells and limited types of vertices. On the contrary, all vertices should be generally evaluated by conventional methods.

Furthermore, Figure 6 shows distribution patterns of nonzero entries (i.e., nz) of involved matrices for the four-fold origami shown in Fig. 5(a). For instance, the equilibrium matrix H in Fig. 6(d) is utilized to describe the balance between the internal forces of the members and the external loads [34]. The left zero space of H contains internal mechanism modes, which can effectively predict the motion of a foldable structure [29, 35]. In Fig. 6, the symbol · is utilized to indicate a non-zero entry.



Fi ni
shown in Fig. 5(a): (a-c) adjacency matrices of the subgraphs G_2, G_3, and the graph product $G_2 \square G_3$, (d) equilibrium matrix of the equivalent truss framework denoted by the strong Cartesian product $G_2 \boxtimes G_3$

It is important to point out that, the involved matrices of the origami models can be evaluated from those of the subgraphs in a much easier manner [12, 15]. For example, the adjacency matrix shown in Fig. 6(c) exhibits a

good matrix form and significant regularity. It can be effectively computed from the matrices of the generators of the graph, which are shown in Fig. 6(a-b). In addition, Fig. 6(d) describes the equilibrium matrix of the equivalent truss framework denoted by the strong Cartesian product $G_2 \boxtimes G_3$. Recall that this matrix has a less profile and better distributions of nonzero entries, compared with conventional sparse matrices. This is because graph products for origami structures provide an appropriate element ordering and nodal numbering, which can reduce the profile of involved matrices [12, 13]. Thus, equilibrium matrices, stiffness matrices and other involved matrices can have better forms and numerical properties.
Kinematic analysis shows that this 198×215 equilibrium matrix is severely singular. Thus, in the unfolded

state, the truss structure of the origami pattern has up to 63 internal mechanism modes, whereas six rigid-body motions have been excluded. As a result, because of potential singularity [28, 36-38], it is difficult to fold the origami structures from the fully deployed state along the ideal motion path.
Six-fold origami patterns based on directed graph products

As shown in Fig. 7, two different types of six-fold origami models are generated using the directed graph products described in the previous section. Fig. 7(a) plots an origami with Kresling pattern [11], [39].
Interestingly, it comes from the type I product of two directed graphs $D(1{:}8)P_9$ and $D(1{:}8)G_9$, which indicate

that the members 1-8 of both directed graphs P_9 and G_9 with 9 nodes are in positive directions. In this study, the

notations $D+\text{-}P_n$ and $D+\text{-}G_n$ describe directed path and directed subgraph with n nodes, whereas
$(i, j, k\ t{:}k)$ $(i, j, k\ t{:}k)$
$d\ 1{:}\ 2$ $d\ 1{:}\ 2$

member i, is double, member j is in positive direction and member k_1 to k_2 with increment t, are in negative direction [13].

(a) Kresling pattern (b) Waterbomb pattern
Figure 7 Crease patterns of a six-fold origami expressed by directed graph products and further operations In Fig. 7(b), two directed graph products S_1 and S_2 depict two origami patterns with twist buckling modes [11], given by

$$S_1 = D_{(1:2)}P_3 \times_1 D_{(1:2:5,2:2:6)}P_7 \quad S_2 = D_{(1:2)}P_3 \times_1 D_{(1:2:5,2:2:6)}P_7 \tag{13}$$

, and

where $D_{(1:2)}P_3$ and $D_{(1:2)}P_3$ respectively denote the members 1-2 of the graphs P_3 are in positive and negative directions, and the vertical $D_{(1:2:5,2:2:6)}P_7$ in Fig. 7(b) denotes that the members 1, 3, and 5 are in positive graph directions and the members 2, 4, and 6 are in negative directions. As the directions of the horizontal graphs are different, the diagonal members in the generated patterns are different. Moreover, we utilize the operator for the ring sum of the directed graph products S_1 and S_2. As a result, a different type of origami model with Waterbomb pattern (Chen et al. [7]; Kuribayashi et al. [22]) is developed. As shown in Fig. 7(b), the intersecting line of the two graphs and the involved nodes have been removed.

Notably, by combining with cycles, weighted graphs and subgraphs, we can develop crease patterns for 3D origami structures with complex geometry. As shown in Fig. 8, crease patterns of cylinders associated with the Kresling pattern are studied.

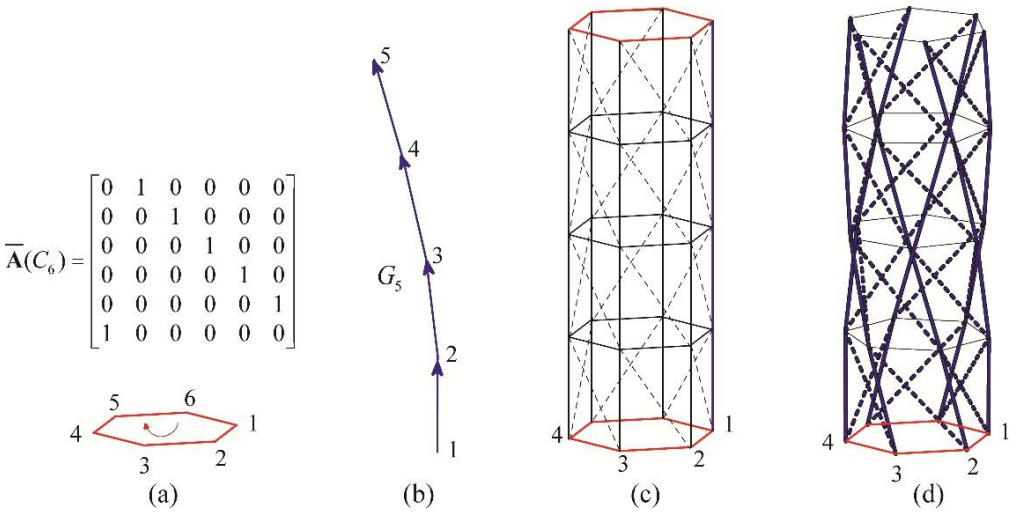


Figure 8 Cylinders expressed by directed graph products of weighted graphs in 3D space: (a) a directed cycle $D_{1:6+}C_6$ and its modified adjacency matrix $\overline{A}(C_6)$; (b) a weighted graph $D_{1:4+}C_5$ in 3D space; (c) a typical cylinder obtained by $D_{1:6+}C_6(\prime)_1 D_{1:4+}P_5$; (d) a twisted cylinder with the Kresling pattern generated by $D_{1:6+}C_6(\prime)_1 D_{1:4+}G_5$

Conventional cylinders such as the one shown in Fig. 8(c) can be directly generated from the directed cycle and path graphs, given by

$$S = D_{1:6} C_6 (-)_1 D_{1:4} P_5 \quad (14)$$

where the geometry of the graphs is not integrated. In fact, as shown in Fig. 8(d), a specific cylinder with the Kresling pattern can be obtained by twisting a conventional thin cylinder [11, 39, 40]. It retains cyclic symmetry [41, 42], and keeps equivalent under proper rotations along the principal axis. Its crease pattern can be accurately established by

$$S = D_{1:6} C_6 (-)_1 D_{1:4} G_5 \quad (15)$$

where the subgraph G_5 is a directed weight graph in 3D space. Based on Eq. (11), the coordinates of each node of the graph are wriiten as

$$N = G = [x \quad y \quad z]^T = [r\cos(i\alpha + \beta i) \quad r\sin(i\alpha + \beta i) \quad (i-1)h]^T, \quad i \in [1, 5] \quad (16)$$

i 5 *i* *i* *i* *t* *t*

where r is the radius of the cylinder, $\square_t$ is the twisted angle between the layers of the cylinder, h is the height of one layer, and they satisfy [40]

$$h \square r\square_t \tan(\square) \quad (17)$$

In Eq. (17), $\square$ is the angle between the weighted graph shown in Fig. 8(b) and the horizontal plane, and $\square_t$ indicates the twisted state of the cylinder with the Kresling pattern [40]. For instance, $\square = 0$ when the cylinder is folded. It is important to point out that Eq. (17) is based on infinitesimal bar stretching assumption (i.e., undeformed bar length is utilized to describe the global geometry of the structure).

Based on the graph product computed by Eq. (15) and the FEM analysis using ABAQUS, the equivalent truss framework of the twisted cylinder with the Kresling pattern (see Fig. 8d) is investigated to study the deformation process. Figure 9 illustrates four typical configurations of the cylinder in the deformation process, where r =1000mm and h = 1200mm at the initial configuration. It shows that this cylinder can be fully folded from the initial configuration, where the bar members get stresses when deformed. Notably, the deformation process agrees well with the results presented by Cai et al. [40]. Therefore, the proposed graph products provide a good choice for numerical models or finite element modeling of the origami structures.

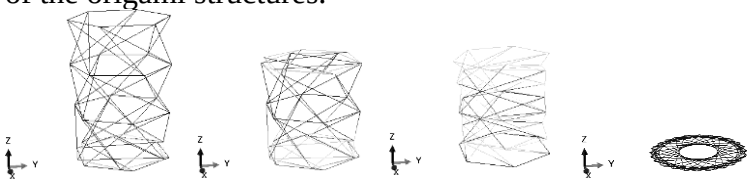


Figure 9 Deformation process of truss framework of a cylinder with the Kresling pattern

Conclusions and Discussions

Using undirected and directed graph products, we can describe a large variety of origami patterns (e.g., the Miura pattern, different four-fold patterns, Kresling pattern, and Waterbomb pattern), and easily construct the involved matrices and simplified structural models of these structures. On the basis of the graph products and the properties of their generators, the topological properties of origami models can be evaluated in a much easier

manner. For example, the adjacency matrices of the models can be computed from those of their generators. Furthermore, the presented method can be extended to the formation of other types of structures and their numerical models. Using different operators of graph products, we can obtain the compact representation of origami structures with complex patterns. More importantly, because the graph products and their operators introduced in this study are systematic, computer programs would be easily generated and exploited. Admittedly, the origami patterns described by the present approach are somewhat periodic. Robust methods for more general patterns with complex geometries or non-periodic characters should be concerned in the future study.

References

[1] Yasuda, H., and Yang, J. (2015), "Reentrant origami-based metamaterials with negative poisson's ratio and bistability," Physical Review Letters, 114(18), 185502.
[2] Brunck, V., Lechenault, F., Reid, A., and Adda-Bedia, M. (2016), "Elastic theory of origami-based metamaterials," Physical Review E, 93(3), 033005.
[3] Silverberg, J. L., Evans, A. A., McLeod, L., Hayward, R. C., Hull, T., Santangelo, C. D., and Cohen, I., "Using origami design principles to fold reprogrammable mechanical metamaterials," Science, [4] 345(6197), pp. 647-650, 2014.
[5] You, Z., "Materials design," 2014. Folding structures from flat materials, Science, 345(6197), pp. 623-624.
[6] Chen, Y., Peng, R., and You, Z. (2015), "Origami of thick panels," Science, 349(6246), pp. 396-400.
[7] Chen, Y., Feng, H. J., Ma, J. Y., Peng, R., and You, Z., "Symmetric waterbomb origami," Proceedings of the Royal Society A-Mathematical Physical and Engineering Sciences, 472(2190), 20150846, 2016.
[8] Zhang, X., Cheng, G., You, Z., and Zhang, H., "Energy absorption of axially compressed thin-walled square tubes with patterns," Thin-Walled Structures, 45(9), pp. 737-746, 2007.
[9] Wei, Z. Y., Guo, Z. V., Dudte, L., Liang, H. Y., and Mahadevan, L. (2013), "Geometric mechanics of periodic pleated origami," Physical Review Letters, 110(21), pp. 325-329.
[10] Tachi, T., "Generalization of rigid foldable quadrilateral mesh origami," Journal of the International Association for Shell & Spatial Structures, 50(162), pp. 173-179, 2009.
[11] Kuribayashi, K., Tsuchiya, K., You, Z., Tomus, D., Umemoto, M., Ito, T., and Sasaki, M., "Self-deployable origami stent grafts as a biomedical application of Ni-rich TiNi shape memory alloy foil," Materials Science and Engineering A-Structural Materials Properties Microstructure and Processing, 419(1-2), pp. 131-137.
[12] "Twist buckling and the foldable cylinder: an exercise in origami," International Journal of Non-Linear Mechanics, 40(6), pp. 833-843, Hunt, G. W., and Ario, L. (2005).
[13] Kaveh, A., Optimal analysis of structures using symmetry and regularity ideas, Springer, 2013.
[14] "Graph products for configuration processing of space structures," Computers & Structures, 86(11), pp. 1219-1231, Kaveh, A., and Koohestani, K. (2008).
[15] Kaveh and Rahami, "A unified method for eigendecomposition of graph products," Communications in numerical methods in engineering, 21(7), pp. 377-388, 2005.
[16] Chen, Y., and Feng, J. (2016), "Improved symmetry method for the mobility of regular structures using graph products," Journal of Structural Engineering, 142(9), 04016051.
[17] "A Framework for the symmetric generalisation of the Miura-ori," International Journal of Space Structures, 30(2), pp. 141-152, Sareh, P., and Guest, S. D. (2015).

[18] "Design of isomorphic symmetric descendants of the Miura-ori," Smart Materials and Structures, 24(8), 085001, Sareh, P., and Guest, S. D. (2015).
[19] Kaveh and Nikbakht (2010) "Improved group-theoretical method for eigenvalue problems of special symmetric structures, using graph theory," Advances in Engineering Software, 41(1), pp. 22-31.
[20] "A general theorem for adjacency matrices of graph products and application in graph partitioning for parallel computing," Finite Elements in Analysis and Design, 45(3), pp. 149-155, Kaveh, A., and Alinejad, B. (2009).
[21] Sabidussi, G. "Graph multiplication," Mathematische Zeitschrift, 72(1), pp. 446-457, 1959.
[22] Koohestani, K. (2012), "Exploitation of symmetry in graphs with applications to finite and boundary elements analysis," International Journal for Numerical Methods in Engineering, 90(2), pp. 152-176.
[23] Fan, R. K. C., Spectral graph theory, American Mathematical Society, 1997.
[24] "Designing symmetric derivatives of the Miura-ori," Sareh, P., and Guest, S. D. (2014), Advances in Architectural Geometry, pp. 233-241.
[25] Gattas, J. M., Wu, W., and You, Z. (2013), "Miura-base rigid origami: parameterizations of first-level derivative and piecewise geometries," Journal of Mechanical Design-Transactions of the ASME, 135(11), 0111011.
[26] Tachi, T. (2010). "Geometric considerations for the design of rigid origami structures," International Association for Shell and Spatial Structures (IASS) Symposium Proceedings, pp. 458-460.
[27] "Design of non-isomorphic symmetric descendants of the Miura-ori," Smart Materials and Structures, 24(8), 085002, Sareh, P., and Guest, S. D. (2015).
[28] "Graphs that admit polyline drawings with few crossing angles," SIAM Journal on Discrete Mathematics, 26(1), pp. 305-320, Ackerman, E., Fulek, R., and Th, C. D. (2012).
[29] Chen, Y., Feng, J., and Ren, Z. (2016) "Numerical approach for detecting bifurcation points of the compatibility paths of symmetric deployable structures," Mechanics Research Communications, 71, pp. 7–15.
[30] "Folding of a type of deployable origami structures," International Journal of Structural Stability and Dynamics, 12(6), 1250054, Chen, Y., and Feng, J. (2012).
[31] Filipov, E. T., Liu, K., Tachi, T., Schenk, M., and Paulino, G. H., "Bar and hinge models for scalable analysis of origami," International Journal of Solids and Structures, 124, pp. 26-45, 2017.
[32] Sareh, P. (2014). Miura-ori symmetric descendants, University of Cambridge, UK.
[33] Geometric folding algorithms: links, origami, polyhedra, Demaine, E. D., and O'Rourke, J. (2008), Cambridge University Press.
[34] Akitaya, H., D. Demaine, E., Horiyama, T., Hull, T., Ku, J., and Tachi, T., 2018, "Rigid Foldability is NP-Hard," arXiv:1812.01160.
[35] Chen, Y., Feng, J., Ma, R., and Zhang, Y. (2015), "Efficient symmetry method for calculating integral prestress modes of statically indeterminate cable-strut structures," Journal of Structural Engineering, 141(10), 04014240.
[36] Chen, Y., Fan, L., and Feng, J. (2017) "Kinematic of symmetric deployable scissor-hinge structures with integral mechanism mode," Computers & Structures, 191, 140-152.
[37] Chen, Y., Feng, J., and Sun, Q. (2018) "Lower-order symmetric mechanism modes and bifurcation behavior of deployable bar structures with cyclic symmetry," International Journal of Solids and Structures, 139–140, pp. 1–14.
[38] Silverberg, J. L., Na, J. H., Evans, A. A., Liu, B., Hull, T. C., Santangelo, C. D., Lang, R. J., Hayward, R. C., and Cohen, I., "Origami structures with a critical transition to bistability arising from hidden degrees of freedom," Nature Materials, 14(4), pp. 389-393, 2015.
[39] Waitukaitis, S., Menaut, R., Chen, B., and van Hecke, M. (2015), "Origami multistability: from single vertices to metasheets," Physical Review Letters, 114(5), 055503.

[40] Kresling, B., "Natural twist buckling in shells: from the Hawkmoth's bellows to the deployable kresling-pattern and cylindrical Miura-Ori" (2008), 6th International Conference on Computation of Shell & Spatial Structures (IASS-IACM 2008), Ithaca, NY, May 28-31.
[41] Cai, J., Deng, X., Zhang, Y., Feng, J., and Zhou, Y. (2016), "Folding behavior of a foldable prismatic mast With Kresling origami pattern," Journal of Mechanisms & Robotics-Transactions of the ASME, 8, 031004.
[42] Chen, Y., and Feng, J. (2012) "Generalized eigenvalue analysis of symmetric prestressed structures employing